Published in final edited form as:
Radiology. 2007 July ; 244(1): 130–137.

Detection of simulated microcalcifications in a phantom with digital mammography: effect of pixel size

Sankararaman Suryanarayanan, Ph.D.M.B.A.[1,2], **Andrew Karellas, Ph.D.**[1,2], **Srinivasan Vedantham, Ph.D.**[1], **Ioannis Sechopoulos, M.S.**[1,2], and **Carl J D'Orsi, M.D.**[1]

1 *Winship Cancer Institute and Department of Radiology Emory University School of Medicine Atlanta, GA 30322, USA*

2 *Wallace H. Coulter Department of Biomedical Engineering at Georgia Institute of Technology and Emory University Atlanta, GA 30332, USA*

Abstract

PURPOSE—To evaluate the effect of pixel size on the detection of simulated microcalcifications in digital mammography using a phantom.

MATERIALS AND METHODS—A high-resolution prototype imager with variable pixel size of 39 and 78 μm, and a clinical full-field digital mammography (FFDM) system with pixel size of 100 μm were used. X-ray images of a contrast-detail (CD) phantom were obtained to perform alternative forced choice (AFC) observer experiments. Polymethyl-methacrylate (PMMA) was added to obtain phantom thickness of 45 and 58 mm which are typical breast thickness conditions encountered in mammography. Phantom images were acquired with both systems under nearly identical exposure conditions using an anti-scatter grid. Twelve images were acquired for each phantom thickness and pixel size (total of 72 images) and six observers participated in this study. Observer responses were used to compute the fraction of correctly detected disks. A signal detection model was used to fit the recorded data from which CD characteristics were obtained. Repeated-measures analyses using mixed effects linear models were performed for each of the 6 observers. All statistical tests were 2-sided and unadjusted for multiple comparisons. A P value of 0.05 or less was considered to indicate statistical significance.

RESULTS—Statistical analysis indicated significantly better CD characteristics with 39 and 78 μm pixel sizes compared to the 100 μm pixel for all disk diameters and phantom thickness conditions ($p<0.001$). Increase in phantom thickness degraded CD characteristics irrespective of pixel size ($p<0.001$).

CONCLUSION—Based on the conditions of this study, reducing pixel size below 100 μm with low imaging system noise enhances the visual perception of small objects that correspond to typical microcalcification size.

Corresponding author: Andrew Karellas Ph.D., Professor of Radiology, Hematology, and Oncology, Director of Medical Physics, Department of Radiology, Emory University School of Medicine, Winship Cancer Institute, 1701 Uppergate Drive, Building C, Suite 5018, Atlanta, GA 30322., Email: akarell@emory.edu, Phone: (404) 712 2411, FAX: (404) 712 5813.

Advances in Knowledge: The results of this study indicate superior performance of 39 and 78 μm pixel sizes (high-resolution prototype digital imager) compared with 100 μm pixel size (clinical FFDM system).

Implications for Patient Care: Based on the conditions investigated in this study, it appears that high-resolution (below 100 μm pixel size) and low-noise digital x-ray mammography systems could potentially improve the detection and visualization of microcalcifications leading to early and more accurate diagnosis.

The results of a large-scale clinical study involving a variety of digital mammography systems indicated that the overall diagnostic accuracy of full-field digital mammography (FFDM) and screen-film mammography (SFM) as a means of screening for breast cancer was similar (1). However, the study also reported that digital mammography was more accurate in women under the age of 50, women with radiographically dense breasts, and premenopausal or perimenopausal women (1). Despite the advantages of FFDM over SFM, the relative performance of digital mammography compared to film for specific types of features, particularly for very subtle microcalcifications, remains to be established. The large-area contrast properties of FFDM suggest that its ability to detect soft tissue masses and architectural distortions is likely to exceed that of film but it is not quite as clear whether this holds true for the detection of microcalcifications. Several studies have demonstrated that the presentation of ductal carcinoma in situ (DCIS) mammographically is by microcalcifications alone in up to 72% of instances (2-5). Berg et al. (6) found that 20% of biopsies for amorphous calcifications were malignant. These calcifications are at the threshold of visibility and any parameter that increases their detection is important. The larger effective pixel size in digital mammography and the resulting lower spatial resolution compared to SFM warrants particular attention for the optimization of FFDM systems with respect to detectability of subtle microcalcifications.

Currently there is no consensus on the desirable pixel size or spatial resolution for digital mammography systems. Clinical amorphous silicon (a-Si:H)-based FFDM systems have a pixel size of 100 μm (7,8) and amorphous selenium (a-Se)-based clinical FFDM systems have a pixel size of 70 μm (9). Smaller pixel sizes in digital mammography is offered by a slot-scan system based on charge coupled device (CCD) technology (10) and a photon counting detector system in a slot scan geometry (11,12). In addition, smaller spatial sampling is offered by photostimulable storage phosphor technology (13).

Various studies point to the possible need for higher spatial resolution in digital mammography (14–17). Yamada and colleagues (16) concluded that high spatial resolution is required in digital mammography to successfully differentiate between microcalcifications. Ruschin *et al.* (17) found improved performance in terms of microcalcification shape determination at pixel sizes well below 100 μm. The pixel size of current large area flat-panel digital mammography imagers has a range of 70–100 μm, but knowledge on the performance of smaller pixels is limited. However, current flat panel-based systems using a-Si:H or amorphous selenium (a-Se) detectors cannot be used to study the effect of small pixel because pixel sizes of about or below 50 μm are currently not available. The purpose of our study was to evaluate the effect of pixel size on the detection of simulated microcalcifications in digital mammography using a phantom.

MATERIALS AND METHODS

Clinical FFDM System

A clinical full-field digital mammography system (Senographe 2000D, GE Medical Systems, Milwaukee, WI) was used to acquire the 100 μm images for this study (7,8). The system comprises a columnar cesium iodide (CsI:Tl) scintillator coupled to an a-Si:H photodiode array with a pixel size of 100 μm providing a field of view of 19 × 23 cm.

Prototype FFDM System

A 16 × 24-cm laboratory prototype FFDM imager was developed based on CCD technology (Fairchild Imaging Inc., Milpitas, CA) (18,19). The imager was constructed by assembling 6 solid-state monolithic CCD modules of size 8 × 8-cm where each monolithic CCD module was designed to be 3-side buttable with each module comprising 2048 × 2048 pixels. The imaging device could be operated at 39 and 78 μm pixel modes with unity fill factor. The CCD

design incorporated a full-frame architecture. Each CCD module was directly coupled to a non-tapering fiber optic faceplate (Schott North America Inc., Southbridge, MA). A CsI:Tl scintillator of dimension ~16 × 24 cm with a thickness of 150-μm deposited on an amorphous carbon substrate (Hamamatsu Corporation, Bridgewater, NJ) was placed on the fiber optic face plate. A foam-type material was placed over the scintillator substrate and the complete assembly was pressure bonded with a detector cover plate. The detector and electronics were enclosed in a cassette like format and operated without liquid circulation for cooling.

Contrast Detail Phantom

A contrast-detail (CD) phantom (CDMAM 3.2, Fluke Biomedical, Cleveland, OH), originally developed by Thijssen and colleagues was used as the test object in this study (20). This phantom has been widely used for image quality assessment in mammography. The phantom consists of a thin aluminum base that contains circular gold disks that are logarithmically sized from 0.10 to 3.2 mm in diameter and 0.05 to 1.6 μm in thickness. The disks are arranged in a matrix of squares such that, within each square, one disk is centrally placed and an additional disk is randomly placed at one of the four corners. Within each square, the central and corner disks have the same diameter and thickness. Along a row of squares, the disk thickness is constant while logarithmically varying in diameter and along a column the diameter remains constant while the thickness varies logarithmically (21). For the purpose of this study additional polymethyl-methacrylate (PMMA) was added such that the total physical thickness of the phantom was 45 and 58 mm respectively. The main advantage of this phantom is the presence of a randomly spaced corner disk in each square that facilitates alternative forced choice experiments. It has recently been shown that for mammographic features smaller than 1 mm in size, such as microcalcifications, the quantum and electronic noise characteristics of the imaging system are overwhelmingly dominant compared to the anatomic structural noise of the breast (22). Therefore, it is appropriate to perform CD analysis using a phantom without the anatomic noise that is encountered in a mammographic image. This phantom has been used previously to compare CD characteristics of a SFM and FFDM system (23).

Image Acquisition

Images of the CDMAM phantom were first acquired using the clinical FFDM system (Senographe 2000D, GE Medical Systems, Milwaukee, WI) in the “contrast auto” mode for emphasis on image contrast. The compression paddle and the anti-scatter grid were used to simulate a clinical situation. The mammography system automatically selected kVp, mAs, target/filter for both phantom thickness conditions. For each phantom thickness condition 12 images were acquired at 100 μm pixel resolution and the raw images were selected for this study. The raw images were automatically bad-pixel and flat-field corrected by the clinical FFDM system. The prototype FFDM imager was used with an older mammography unit (Senographe DMR, GE Medical Systems, WI) with a source-to-detector distance (SID) of 66 cm identical to the clinical FFDM system. A reciprocating anti-scatter grid with a grid ratio of 5:1 was used during image acquisition. The images were acquired with both mammography units under nearly identical exposure conditions (Table 1). As with the clinical system, 12 images were acquired for each phantom thickness (45 and 58 mm) and pixel condition (39 and 78 μm). The images were dark subtracted, flat-field, and bad-pixel corrected by one of the authors (S.S.) by implementing a computer program. Disk diameters between 0.13 to 0.31 mm were used in this study. For each disk diameter, six disk thickness levels were selected such that disk perception ranged from ‘marginally’ to ‘easily’ perceivable.

Image Processing and Display

A graphical user interface (GUI) program was developed by author S.S. using Interactive Data Language (IDL 6.0, Research Systems Inc, Boulder, CO). The squares in the phantom images

that corresponded to the disk diameters and thickness of interest were cropped before display using a computer program by one of the authors (S.S.). The dimensions of the region of interest (ROI) for the 100 μm, 78 μm, and 39 μm pixel sizes were 100 ×100, 130 × 130, and 260 × 260 pixels respectively. All image ROIs were displayed in the center of a DICOM calibrated clinical gray scale flat-panel display system (DOME C5i, Beaverton, OR). No zooming was performed to match the ROI sizes. Since there were 5 disk diameters, 6 disk thickness, and 12 images per condition, 360 image ROIs were displayed to the observer for each phantom thickness and pixel condition. Visual cues were generated by the display program at each of the four corners of the square where one of the corners contained the disk. Each displayed ROI was adjusted using an automatic contrast enhancement technique. In order to achieve this, histogram analysis was performed to compute the density function of each ROI with maximum value set to the maximum digital value in that ROI image. The digital value corresponding to the peak of the histogram (also in digital units) was obtained and the look-up table of the image display was scaled such that threshold was set to be greater than half this value (Fig 1). A reference image ROI that contained a high contrast version of the disk in the center was displayed above the image ROI in order to provide the observer with information related to the detection task. The diameter of the disk in reference image always matched the diameter of the disk in the image ROI. However, none of the observers were aware of the disk diameters and the type of image ROI being displayed during the observation sessions. An automated messaging feature was implemented that indicated to the observer when 25, 50, 75, and 100% of the observation session was completed.

Observer Study

A total of 6 observers that included four board certified radiologists with specialization in mammography and two graduate students with experience in medical imaging participated in this study. The experience of the four radiologists in mammography was 4, 7, 14, and 34 years. The two graduate students had 3 and 4 years of experience in medical physics and radiology research. Two of the authors (C.J.D. and I.S.) participated as observers in the study. The study was divided into six sessions in random order. On a given day each observer was expected to complete two sessions. It took three visits per observer to complete the whole study. In each session, observers had to independently review 360 image ROIs which on average took about 25–30 min. For the complete study across all six sessions each observer reviewed 360 × 6 = 2160 image ROIs. Before commencing each session, observers were trained with a small random subset of ROI images (~15–20 ROIs for each condition) extracted from the acquire images until they felt comfortable with the task. Since the type of image ROI, display sequence, and position of the disk in each ROI were all random the chances of learning or memory effects were virtually eliminated. No restrictions on viewing distance were placed but the observers were not allowed to window/level the image ROIs. All observations were conducted in a dedicated darkened radiologic image perception room and randomized between observers to minimize any systematic effects. Since this was a forced choice study, an observer had to indicate the location of the corner disk with a mouse click and was encouraged to arrive at the best estimate in cases where the disk was not perceivable. Observer responses were automatically recorded as true positive (TP) or false positive (FP) events and used to compute ‘percent correct detection’.

Data Analysis

Based on the recorded observer responses, ‘percent correct detection’, Pc (sensitivity) values were computed for each observer, disk diameter, and thickness. To analyze the ‘percent correct detection’ data, a signal detection model was used that hypothesizes a continuous decision variable internal to the observer with Gaussian probability density functions for the presence or absence of the disk (24,25). A maximum-likelihood algorithm was implemented as described in detail by Ohara et al (24) to fit the detection data. The CD characteristics were obtained at

the 62.5% detection threshold level as this provided a threshold between 'chance' (25%) and 100% correct detection. For each observer and diameter the perceived disk thickness corresponding to the 62.5% correct detection threshold point in the detection curve was computed. Linear interpolation of adjacent points was performed wherever applicable. Contrast-detail characteristics were derived for all diameters, observers, and phantom thickness conditions. Finally, the corresponding CD data from individual observers were averaged in order to obtain average CD characteristics.

Statistical Analysis

Repeated-measures analyses using mixed effects linear models were performed for the perceived disk thickness outcome as measured by each of the 6 observers. A saturated model was fit that included the fixed main effects (phantom thickness, pixel size, and diameter), the two-way statistical interaction including thickness by pixel size, thickness by diameter, pixel size by diameter, and the three-way interaction including thickness by pixel size by diameter. The analyses were performed using a means model by using SAS Proc Mixed (version 8, SAS Institute, Cary, NC), providing separate estimates of perceived mean disk depth by thickness, pixel size and disk diameter. A compound-symmetry variance-covariance form in observer measurements was assumed for perceived disk depth and robust estimates of the standard errors of parameters were used to perform statistical tests and construct 95% confidence intervals. All statistical tests were 2-sided and unadjusted for multiple comparisons. A P value of 0.05 or less was considered to indicate statistical significance.

RESULTS

Overall, the computed Pc characteristics indicated degradation in detection with increasing pixel size (Figs 2a and 2b) under the conditions investigated. The mean perceived disk thickness for the 45 and 58 mm thick phantom changed in significantly different ways across pixel size and disk diameter ($P < 0.0001$, for the 3-way interaction thickness X pixel size X disk diameter; the 2-way interactions were $P = 0.30$ for thickness X pixel size, $P < 0.0001$ for pixel size X disk diameter, and $P < 0.0001$ for thickness X disk diameter). For the 45 mm thick phantom, perceived disk thickness for both 39 and 78 μm pixel sizes was statistically significant (better threshold contrast) compared to the 100 μm pixel at each disk diameter (Fig 3a, Table 2). The perceived disk thickness was worse for the 78 μm pixel size compared to the 39 μm pixel at disk diameters of 0.13 and 0.16 mm but not for disk diameters of 0.20, 0.25, and 0.31 mm (Fig 3a), indicating superior performance of the 39 μm pixel at 0.13 and 0.16 mm disk diameters (Table 2). For the 58 mm thick phantom, the perceived disk thickness at 39 and 78 μm pixel sizes were statistically significant compared to the 100 μm pixel (Fig 3b, Table 3). The perceived disk thickness was worse for the 78 μm pixel size compared to the 39 μm pixel size (Fig 3b) at disk diameter 0.13 mm, the perceived disk thickness was statistically significant for the 78 μm pixel size compared to the 39 μm pixel at disk diameter 0.16 mm ($P = 0.04$) and the mean perceived disk thickness was similar for the 78 μm and 39 μm pixel sizes at disk diameters 0.20 and 0.25 mm (Table 3). However, the difference between the mean perceived disk thickness at disk diameter 0.16 mm is statistically significant but the magnitude of this difference is small. On average, perceived disk thickness for all pixel sizes was statistically better for the 45 mm phantom compared to the 58 mm thick phantom (Fig 4) at each of the five disk diameters (Table 4).

DISCUSSION

The use of CD methodology for the evaluation of clinical imaging systems is widely accepted and such psychophysical characterization of imaging systems provides information on the image quality and diagnostic value of a modality (26,27). The methodology described in our

study provides a means to quantitatively assess perception data and characterize imaging performance. Various investigators have successfully used similar approaches to assess image quality in x-ray imaging (21,26–34). An important factor that motivates CD analysis is the inclusion of the human observer as part of the imaging chain, which is a critical consideration in all medical imaging systems (35). Contrast-detail methodology can be extremely useful as a precursor study before clinical trials, to determine system performance or compare the performance among different systems in a controlled manner. Contrast-detail analysis may reveal strengths or deficiencies in a system that may need correction before the onset of comprehensive clinical studies. The logistics and cost considerations present significant barriers in the evaluation of specific parameters through clinical trials. Hence, studies such as this can be very instructive in gaining a quantitative understanding of performance before embarking on redesign of mammography systems or on comprehensive clinical trials. Other automated methods (36,37) can also be used in combination with human observers to analyze system performance.

We focused on obtaining a quantitative comparison of imaging performance for detection of simulated microcalcifications between two systems at various pixel sizes. However, a combination of pixel size and system noise is likely to have had an effect on the CD characteristics. The alternative forced choice (AFC) method used here provides an effective means of conducting psychophysical measurements (38). In our investigation, the random signal location is likely to have mitigated observer learning bias to a great extent compared to more simplistic CD experiments where the location of the signal is fixed. The superior CD performance of the prototype system at 39 and 78 μm pixel sizes compared to the clinical FFDM system at 100 μm can be attributed to the better $MTF(f)$ and $DQE(f)$ characteristics of the prototype imager especially at higher spatial frequencies (18). However, there are other means of improving the conspicuity of small high frequency structures such as microcalcifications through post-acquisition image processing techniques. The CD performance of the prototype at both 45 and 58 mm phantom thickness conditions demonstrates the viability of such imaging architectures for digital mammography.

The significantly better CD performance of the 39 μm pixel compared to the 78 μm pixel for the 45 mm thick phantom at disk diameters 0.13 and 0.16 mm demonstrates the resolving capability of small pixel sizes under the image noise conditions investigated. Similar rationale holds good for the better performance of the 39 μm pixel for the 58 mm thick phantom at disk diameter 0.13 mm. The unexpected reversal of performance at disk diameter 0.16 mm for the 58 mm thick phantom wherein the 78 μm pixel performed better is primarily due to one observer who exhibited a much higher (poorer) detection threshold for the 39 μm pixel. However, the magnitude of this difference is small. At larger disk diameters, under similar system noise conditions, it appears that the benefit of having small pixel size is reduced. The degradation in detection and CD characteristics between the 45 and 58 mm thick phantom could be attributed to the differences in spectra and possible increase in x-ray scatter that could have potentially impacted the visualization of small low contrast objects irrespective of pixel size.

Our study has limitations. Although ours was not a clinical study with human subjects, the results demonstrate the viability and provide insights into the perceptual performance characteristics of large-area high-resolution imagers for microcalcification detection in the breast. Further, since the effect of breast anatomic noise on microcalcification detection is minor (22), the general trends obtained in this study are clinically relevant. However, a carefully designed clinical study may be required before making a decision on a final pixel size for a specific imaging technology for mammography. The CCD imager in this study was used as a convenient platform to demonstrate the potential of high-resolution and low noise digital mammography for microcalcification detection. Ideally, using the same imager with multiple pixel sizes would have been preferred but such an imager was not available. It should also be

noted that the results of our study are applicable to 2D projections as presently practiced in mammography and studies need to be conducted to explore the resolution and noise effects for applications such as tomosynthesis and dedicated computed tomography of the breast.

Practical application

Based on the conditions of this study, reducing pixel size below 100 μm with low imaging system noise enhances the visual perception of small objects that correspond to typical microcalcification sizes. Alternatively, enhancement of the system modulation transfer function through improved scintillator and detector technologies can enhance microcalcification visualization. We believe our results can help in assessing the performance of similar imaging modalities for x-ray imaging. The CD analysis provides a means to compare and identify key parameters that influence system performance using human observers. The methodology described here can be used before the onset of clinical trials to obtain insights into an imaging system's performance capability for a specific task.

Acknowledgements

The authors thank Kirk A. Easley, MS, Department of Biostatistics, Rollins School of Public Health, Emory University, Atlanta, GA, for assistance with statistical analysis. This study was supported in part by the National Institutes of Health (NIH) grants (R01-CA88792 and R01-EB002123) from the National Cancer Institute (NCI) and the National Institute of Biomedical Imaging and Bioengineering (NIBIB). This work was also supported in part by an infrastructure grant from the Georgia Cancer Coalition (GCC). The contents are solely the responsibility of the authors and do not necessarily represent the official views of the NIH, NCI, NIBIB or the GCC.

References

1. Pisano ED, Gatsonis C, Hendrick E, Yaffe M, Baum JK, Acharyya S, Conant EF, Fajardo LL, Bassett L, D'Orsi CJ, Jong R, Rebner M. Diagnostic performance of digital versus film mammography for breast-cancer screening. N Engl J Med 2005;353:1773–1783. [PubMed: 16169887]
2. Ikeda DM, Andersson I. Ductal carcinoma in situ: atypical mammographic appearances. Radiology 1989;172:661–666. [PubMed: 2549563]
3. Stomper PC, Connolly JL, Meyer JE, Harris JR. Clinically occult ductal carcinoma in situ detected with mammography: analysis of 100 cases with radiologic-pathologic correlation. Radiology 1989;172:235–241. [PubMed: 2544922]
4. Stomper PC, Connolly JL. Mammographic features predicting an extensive intraductal component in early-stage infiltrating ductal carcinoma. American Journal of Roentgenology 1992;158:269–272. [PubMed: 1309620]
5. Kinkel K, Gilles R, Feger C, Guinebretiere JM, Tardivon AA, Masselot J, Vanel D. Focal areas of increased opacity in ductal carcinoma in situ of the comedo type: mammographic-pathologic correlation. Radiology 1994;192:443–446. [PubMed: 8029412]
6. Berg WA, Arnoldus CL, Teferra E, Bhargavan M. Biopsy of amorphous breast calcifications: pathologic outcome and yield at stereotactic biopsy. Radiology 2001;221:495–503. [PubMed: 11687695]
7. Vedantham S, Karellas A, Suryanarayanan S, Albagli D, Han S, Tkaczyk EJ, Landberg CE, Opsahl-Ong B, Granfors PR, Levis I, D'Orsi CJ, Hendrick RE. Full breast digital mammography with an amorphous silicon-based flat panel detector: physical characteristics of a clinical prototype. Med Phys 2000;27:558–567. [PubMed: 10757607]
8. Suryanarayanan S, Karellas A, Vedantham S. Physical characteristics of a full-field digital mammography system. Nucl Instrum Methods Phys Res A 2004;533:560–570.
9. Saunders RS Jr, Samei E, Jesneck JL, Lo JY. Physical characterization of a prototype selenium-based full field digital mammography detector. Med Phys 2005;32:588–599. [PubMed: 15789606]
10. Tesic MM, Fisher Piccaro M, Munier B. Full field digital mammography scanner. Eur J Radiol 1999;31:2–17. [PubMed: 10477093]
11. Aslund M, Cederstrom B, Lundqvist M, Danielsson M. Scatter rejection in scanned multislit digital mammography. Proc SPIE 5368 2004:478–487.

12. Hemdal B, Herrnsdorf L, Andersson I, Bengtsson G, Heddson B, Olsson M. Average glandular dose in routine mammography screening using a Sectra MicroDose mammography unit. Radiat Prot Dosimetry 2005;114:436–443. [PubMed: 15933152]
13. Seibert JA, Boone JM, Cooper VN, Lindfors KK. Cassette-based digital mammography. Technol Cancer Res Treat 2004;3:413–427. [PubMed: 15453806]
14. Cowen AR, Launders JH, Jadav M, Brettle DS. Visibility of microcalcifications in computed and screen-film mammography. Phys Med Biol 1997;42:1533–1548. [PubMed: 9279904]
15. Rong XJ, Shaw CC, Johnston DA, Lemacks MR, Liu X, Whitman GJ, Dryden MJ, Stephens TW, Thompson SK, Krugh KT, Lai CJ. Microcalcification detectability for four mammographic detectors: flat-panel, CCD, CR, and screen/film. Med Phys 2002;29:2052–2061. [PubMed: 12349926]
16. Yamada T, Ishibashi T, Sato A, Saito M, Saito H, Matsuhashi T, Takahashi S. Comparison of screen-film and full-field digital mammography: image contrast and lesion characterization. Radiat Med 2003;21:166–171. [PubMed: 14514123]
17. Ruschin M, Hemdal B, Andersson I, Borjesson S, Hakansson M, Bath M, Grahn A, Tingberg A. Threshold pixel size for shape determination of microcalcifications in digital mammography: a pilot study. Radiat Prot Dosimetry 2005;114:415–423. [PubMed: 15933149]
18. Suryanarayanan S, Karellas A, Vedantham S, Onishi SK. High-resolution imager for digital mammography: physical characterization of a prototype sensor. Phys Med Biol 2005;50:3957–3969. [PubMed: 16177523]
19. Suryanarayanan S, Karellas A, Vedantham S, Sechopoulos I. Theoretical analysis of high-resolution digital mammography. Phys Med Biol 2006;51:3041–3055. [PubMed: 16757861]
20. Thijssen, MAO.; Biijerk, KR.; Lindeyer, JM. Project: Quality Assurance in Mammography (QAMAM). Department of Diagnostic Radiology, University Hospital Nijmegen; St. Radboud, The Netherlands:
21. Veldkamp WJ, Thijssen MA, Karssemeijer N. The value of scatter removal by a grid in full field digital mammography. Med Phys 2003;30:1712–1718. [PubMed: 12906188]
22. Burgess AE. Effect of detector element size on signal detectability in digital mammography. Proc SPIE 5745 2005:232–242.
23. Suryanarayanan S, Karellas A, Vedantham S, Ved H, Baker SP, D'Orsi CJ. Flat-panel digital mammography system: contrast-detail comparison between screen-film radiographs and hard-copy images. Radiology 2002;225:801–807. [PubMed: 12461264]
24. Ohara K, Doi K, Metz CE, Giger ML. Investigation of basic imaging properties in digital radiography. 13. effect of simple structured noise on the detectability of simulated stenotic lesions. Med Phys 1989;16:14–21. [PubMed: 2646515]
25. Aufrichtig R. Comparison of low contrast detectability between a digital amorphous silicon and a screen-film based imaging system for thoracic radiography. Med Phys 1999;26:1349–1358. [PubMed: 10435537]
26. Veldkamp WJH, Kroft LJM, Mertens BJA, Geleijns J. Digital slot-scan charge-coupled device radiography versus AMBER and bucky screen-film radiography: comparison of image quality in a phantom study. Radiology 2005;235:857–866. [PubMed: 15845787]
27. Uffman M, Prokop CS, Neitzel U, Weber M, Herold CJ, Prokop M. Skeletal applications for flat-panel versus storage-phosphor radiography: effect of exposure on detection of low-contrast details. Radiology 2004;231:506–514. [PubMed: 15128995]
28. Hall TJ, Insana MF, Harrison LA, Soller NM, Schlehr KJ. Ultrasound contrast-detail analysis: a comparison of low-contrast detectability among scanhead designs. Med Phys 1995;22:1117–1125. [PubMed: 7565387]
29. Cohen G, Wagner LK, Amtey SR, Di Bianca FA. Contrast-detail-dose and dose efficiency analysis of a scanning digital and a screen-film-grid radiographic system. Med Phys 1981;8:358–367. [PubMed: 7322059]
30. Aufrichtig R, Xue P. Dose efficiency and low-contrast detectability of an amorphous silicon x-ray detector for digital radiography. Physics in Medicine and Biology 2000;45:2653–2669. [PubMed: 11008963]

31. Chotas HG, Ravin CE. Digital chest radiography with a solid-state flat-panel x-ray detector: contrast-detail evaluation with processed images printed on film hard copy. Radiology 2001;218:679–682. [PubMed: 11230639]

32. Verdun FR, Denys A, Valley JF, Schnyder P, Meuli RA. Detection of low-contrast objects: experimental comparison of single-and multi-detector row CT with a phantom. Radiology 2002;223:426–431. [PubMed: 11997548]

33. Cook LT, Insana MF, McFadden MA, Hall TJ, Cox GG. Comparison of the low-contrast detectability of a screen-film system and third generation computed radiography. Med Phys 1994;21:691–695. [PubMed: 7935205]

34. Wang J, Anderson J, Lane T, Stetson C, Moore J. Contrast-detail characteristic evaluations of several display devices. Journal of Digital Imaging 2000;13(2 Suppl 1):162–167. [PubMed: 10847389]

35. Wang J, Langer S. A brief review of human perception factors in digital displays for picture archiving and communications systems. Journal of Digital Imaging 1997;10:158–168. [PubMed: 9399169]

36. Chakraborty DP, Eckert MP. Quantitative versus subjective evaluation of mammography accreditation phantom images. Med Phys 1995;22:133–143. [PubMed: 7565344]

37. Chan HP, Lo SC, Niklason LT, Ikeda DM, Lam KL. Image compression in digital mammography: effects on computerized detection of subtle microcalcifications. Med Phys 1996;23:1325–1336. [PubMed: 8873029]

38. Burgess AE. Comparison of receiver operating characteristic and forced choice observer performance measurement methods. Med Phys 1995;22:643–655. [PubMed: 7643805]

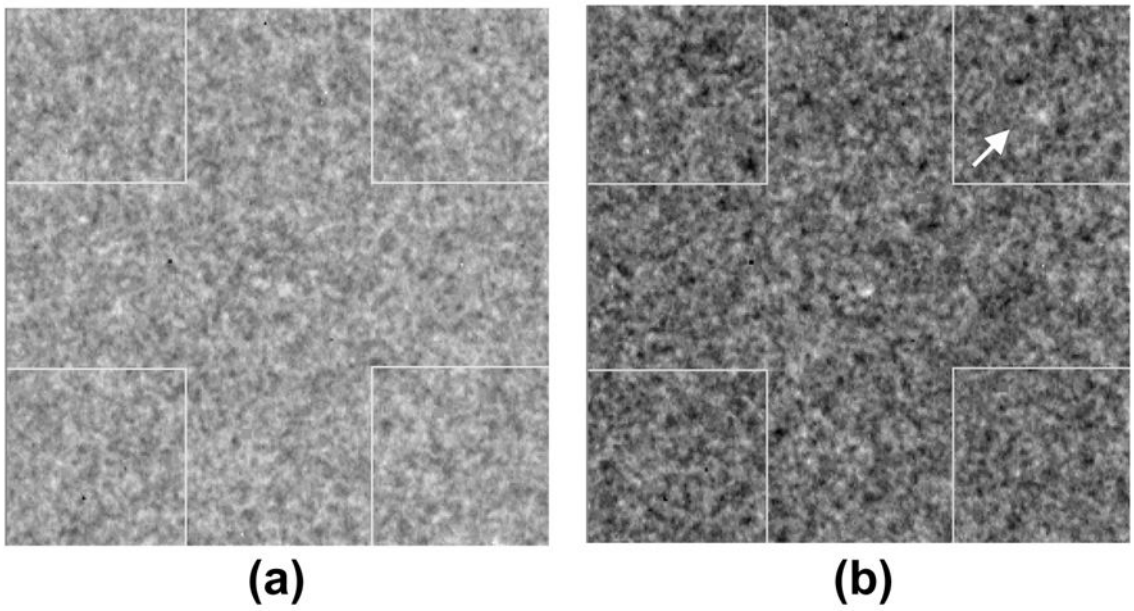

Figure 1.
Image ROI (a) before and (b) after automatic contrast enhancement. Improved visibility of the corner disk is observed after enhancement.

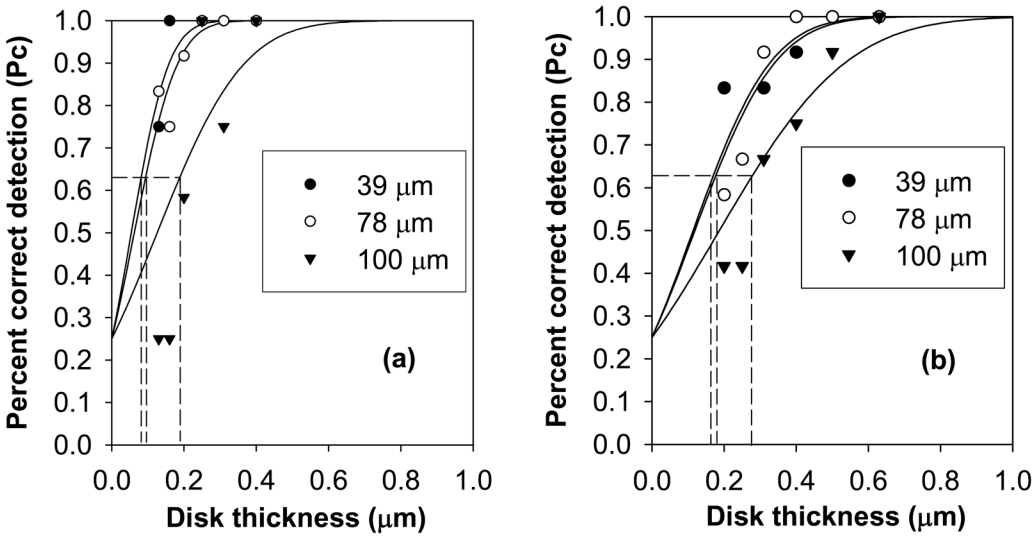

Figure 2.

Examples of percent correct detection (Pc) characteristics obtained from a single observer for disk diameters (a) 0.31 and (b) 0.20 mm at various pixel sizes for a phantom thickness of 45 mm. Degradation in detection with increasing pixel size is observed. The lines are maximum likelihood estimated detection characteristics.

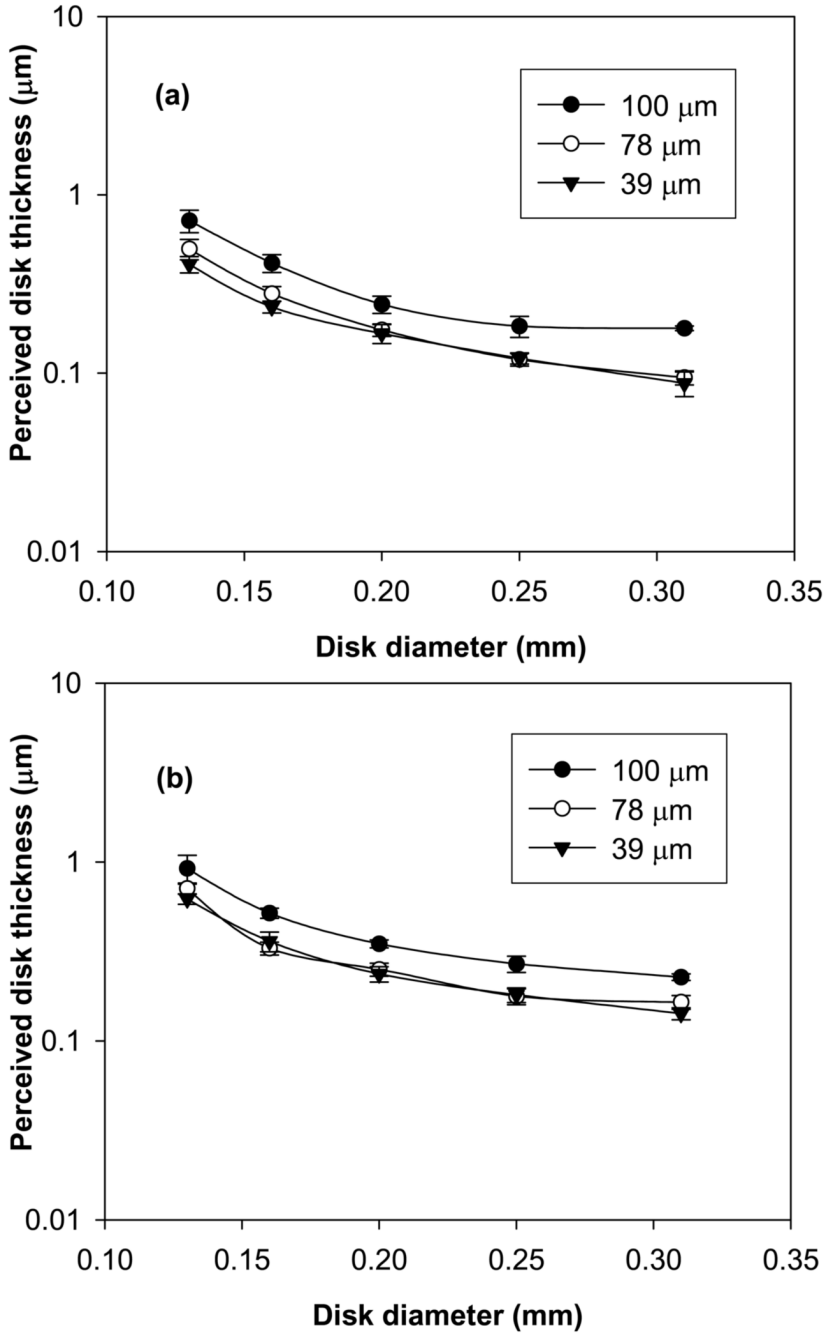

Figure 3.
Contrast-detail (CD) characteristics obtained at 62.5% detection threshold after averaging data from six observers for (a) 45 mm and (b) 58 mm phantom thickness conditions at 39, 78, and 100 μm pixel sizes. Lower (better) threshold CD characteristics at 39 and 78 μm pixel sizes is observed. The error bars indicate 95% confidence interval.

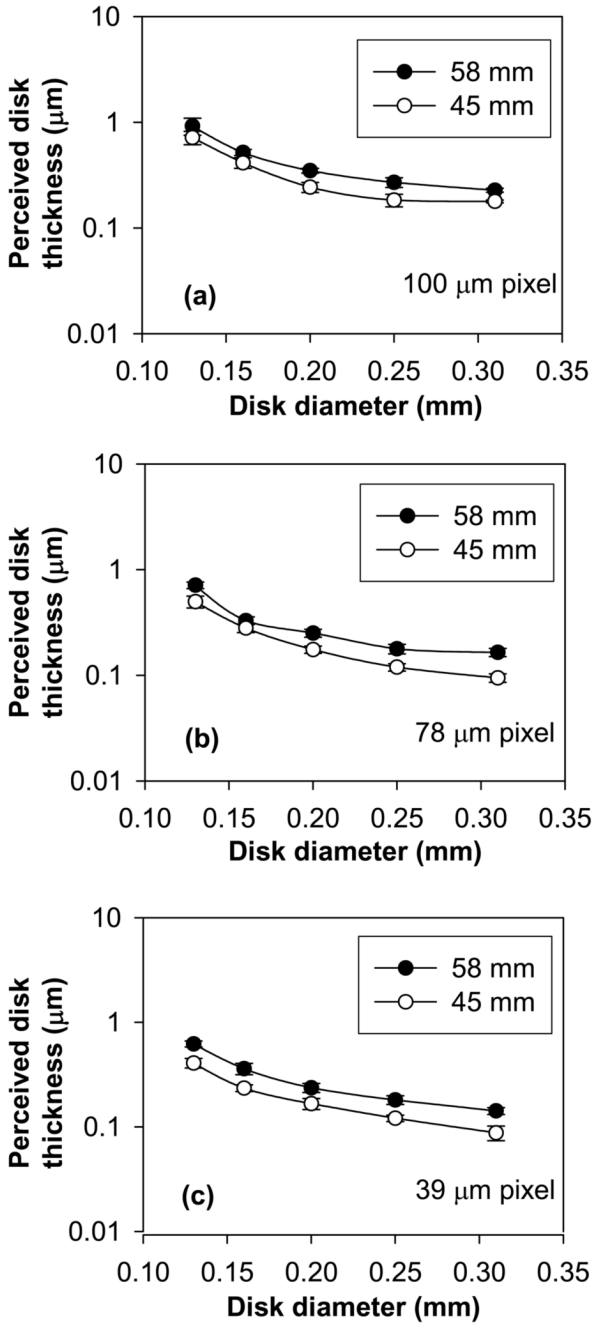

Figure 4.

Contrast-detail (CD) characteristics obtained at 62.5% detection threshold after averaging data from six observers for (a) 100 (b) 78, and (c) 39 μm pixel sizes at 45 and 58 mm phantom thickness conditions. Degradation in CD characteristics irrespective of pixel size is observed. The error bars indicate 95% confidence interval.

TABLE 1

X-ray technique factors and measured imager entrance exposures at 66 cm with no phantom in the beam path for clinical and laboratory mammography units

kVp	Target/filter	Exposure (C/Kg) Clinical x-ray unit	Laboratoty x-ray unit
28	Mo/Mo	0.0006	0.00057
31	Rh/Rh	0.00037	0.00036

TABLE 2

Comparison of the effect of pixel size for a phantom thickness of 45 mm at various disk diameters

Disk diameter (mm)	Pixel size (μm) 100 vs. 78	100 vs. 39	78 vs. 39
0.13	P < 0.0001	P < 0.0001	P < 0.0001
0.16	P < 0.0001	P < 0.0001	P < 0.0001
0.20	P = 0.0003	P = 0.0003	P = 0.10
0.25	P < 0.0001	P < 0.0001	P = 0.77
0.31	P < 0.0001	P < 0.0001	P = 0.19

TABLE 3

Comparison of the effect of pixel size for a phantom thickness of 58 mm at various disk diameters

Disk diameter (mm)	100 vs. 78	Pixel size (μm) 100 vs. 39	78 vs. 39
0.13	P = 0.0045	P = 0.0017	P = 0.003
0.16	P < 0.0001	P < 0.0001	P = 0.04
0.20	P < 0.0001	P < 0.0001	P = 0.09
0.25	P < 0.0001	P < 0.0001	P = 0.59
0.31	P < 0.0001	P < 0.0001	P = 0.05

TABLE 4

Comparison of the effect of phantom thickness (45 vs. 58 mm) for each pixel size at various disk diameters

Disk diameter (mm)	Pixel size (μm) 39	78	100
0.13	P < 0.0001	P < 0.0001	P = 0.026
0.16	P < 0.0001	P = 0.0002	P < 0.0001
0.20	P < 0.0001	P < 0.0001	P < 0.0001
0.25	P < 0.0001	P < 0.0001	P < 0.0001
0.31	P < 0.0001	P < 0.0001	P < 0.0001